Journal of Statistical Physics, Vol. 74, Nos. 5/6, 1994

Relaxation and Transport in FCHC Lattice Gases

D. V. van Coevorden,[1,2] M. H. Ernst,[1] R. Brito,[1,3] and J. A. Somers[4]

Received September 8, 1993; final November 3, 1993

FCHC lattice gases are the basic models for studying flow problems in three-dimensional systems. This paper presents a self-contained theoretical analysis and some computer simulations of such lattice gases, extended to include an arbitrary number of rest particles, with special emphasis on non-semi-detailed balance (NSDB) models. The special FCHC lattice symmetry guarantees isotropy of the Navier–Stokes equations, and enumerates the 12 spurious conservation laws (staggered momenta). The kinetic theory is based on the mean field approximation or the nonlinear Boltzmann equation. It is shown how calculation of the eigenvalues of the linearized Boltzmann equation offers a simple alternative to the Chapman–Enskog method or the multi-time-scale methods for calculating transport coefficients and relaxation rates. The simulated values for the speed of sound in NSDB models slightly disagree with the Boltzmann prediction.

KEY WORDS: Lattice gas automata; transport coefficients; non-detailed balance; staggered invariants; Boltzmann equation.

1. INTRODUCTION

In recent years lattice gas automata (LGCA) as well as the lattice Boltzmann equation defined on the face-centered hypercubic (FCHC) lattice have proven to be useful tools for simulating three-dimensional flow

[1] Institute for Theoretical Physics, University of Utrecht, P.O.B. 80.006, 3508 TA Utrecht, The Netherlands; ernst@ruuntm.fys.ruu.nl.

[2] Permanent address: FOM-Institute for Atomic and Molecular Physics, Kruislaan 407, 1098 SJ Amsterdam, The Netherlands; coevorden@amolf.amolf.nl.

[3] Permanent address: Facultad de CC. Físicas, Universidad Complutense, 28040-Madrid, Spain; brito@seneca.fis.ucm.es.

[4] Koninklijke/Shell-Laboratorium, P.O.B. 3003, 1003 AA Amsterdam, The Netherlands; somers1@ksla.nl.

0022-4715/94/0300-1085$07.00/0

problems.[1-3] Although the choice of four-dimensional FCHC lattice gases to model three-dimensional fluid flow seems rather far-fetched, the point is that there exists no three-dimensional lattice on which fourth-rank tensors are isotropic.[4,5] The isotropy is vital for simulating flow problems, as it implies that the resulting fluid dynamics equations are the isotropic Navier–Stokes equations. Three-dimensional fluids can then be modeled on a four-dimensional lattice by taking only two layers in the fourth dimension combined with periodic boundary conditions. As the algorithms of Somers and Rem[3] for the FCHC lattice can be easily run on workstations, there is a renewed interest in the basic statistical mechanical properties of the FCHC lattice gas. It serves as a starting point for studying three-dimensional surface tension[6] and spinodal decomposition[7] after long-range attractive forces have been added.

In order to increase the efficiency of the implementations of LGCA one has focused on increasing the Reynolds number or decreasing the viscosity, even dropping the physical requirement of positive viscosity coefficients.[1,2] This has been achieved by violating the basic conditions for the existence of the standard local or global equilibrium states. The new stationary states do not satisfy the conditions of detailed balance[8] or the less restrictive Stueckelberg conditions,[9] which are called semi-detailed balance conditions (SDB) in the context of lattice gas cellular automata.[5] These conditions ensure the existence of a universal factorized equilibrium state and of an H-theorem that guarantees the approach of every initial state to this factorized equilibrium, at least within the Boltzmann approximation.[5]

When the Stueckelberg conditions are violated—we refer to such biased models as non-semi-detailed balance (NSDB)—the equilibrium state is not the Gibbs state.[1,2,10] Little is known about the existence and properties of these stationary states. In some NSDB models spatially uniform initial states are unstable[2,11-16] and the systems undergo phase separation. Other models seem to lead to stable uniform equilibrium states, but the velocity distributions do not factorize.[1,2,10]

Violation of SDB gives rise to velocity correlations between the equal-time occupation of different velocity channels at the same or at different nodes in the lattice, both in pre- and postcollision states. In the present paper the existing theory for postcollision correlations[10] will be applied to the FCHC LGCA and compared with computer simulations.

Our main goal is an analytic study of FCHC LGCA which we consider as microscopic N-particle systems, using methods of statistical mechanics and kinetic theory with particular emphasis on the consequences of the lack of SDB. We recall that the concepts of irreversible thermodynamics and linear response theory[7] are based on local equilibrium states being Gibbs states. Within that framework thermodynamic suscep-

tibilities provide exact expressions for the speed of sound and Green–Kubo formulas provide exact expressions for linear transport coefficients in terms of time integrals over time correlation functions, calculated in the Gibbs state. Consequently the lattice gas versions of the Green–Kubo formulas[17] may not be valid for NSDB models.

To obtain approximate results for the transport coefficients we follow the basic ideas of Dubrulle *et al.*,[1] who have applied the assumption of molecular chaos to NSDB LGCA and obtained the Boltzmann equation. When comparing analytic results for FCHC lattice gases with numerical data or with computer simulations we use the biased FCHC model, developed by Somers and Rem,[3,18] and the nonbiased FCHC model, developed by Westland.[19] Recently Grosfils *et al.*[20,21] have studied spatial fluctuations of LGCA in equilibrium. To understand the line shapes and shifts in the dynamic structure factor it is necessary to go beyond terms of order ∇ and ∇^2 in the Navier–Stokes equations, and use the concepts of generalized hydrodynamics and wavenumber-dependent relaxation rates of the Boltzmann equation.[22] In the present paper these quantities will be calculated analytically for FCHC LGCA and evaluated numerically for the Somers–Rem collision rules.

The majority of LGCA are plagued by spurious conservation laws. Here we identify 12 such quantities, present in all FCHC LGCA with or without rest particles. The corresponding conserved quantities satisfy macroscopic equations that couple in a nonlinear fashion to the Navier–Stokes equations.[23,24] In order to understand and control these spurious effects we analyze the conserved densities and calculate the corresponding transport coefficients, called staggered diffusivities. These quantities also enter into the expression for the long-time tail of the stress–stress correlation function.[25]

This paper is organized as follows. Section 2 deals with the special symmetries of FCHC lattices, the Stueckelberg conditions, and spurious invariants. Section 3 and Appendix A discuss the Boltzmann equation and its basic properties. Section 4 gives a theoretical analysis of the eigenvalue spectrum of spatial fluctuations in the Boltzmann equation, and derives explicit expressions for the transport coefficients with details for the bulk viscosity in Appendix B and for the staggered diffusivities in Appendix C. The numerical analysis of the spectral properties appears in Section 5. Computer simulations of sound speed and transport coefficients are compared with kinetic theory and linear response results in Section 6, and we conclude with a discussion.

The theoretical discussions and analysis in the following sections and subsections apply to all FCHC models, as used by the Nice group,[1,2,26] by Somers and Rem,[3,18,19] by Frenkel and co-workers,[27,28] etc. The graphical illustrations and simulations refer to the Somers–Rem model.

2. FCHC MODELS

2.1. Symmetries

FCHC models are defined on the four-dimensional face-centered hypercubic lattice $\mathscr{L}$ with a set of $b = 24$ nearest neighbor lattice vectors $\mathbf{c}_i$ ($i = 1,..., 24$), as listed in Table I. The set of lattice points $\mathbf{r} = \{r_x, r_y, r_z, r_w\}$ is invariant under all cubic symmetry operations $\{S_\alpha, P_{\alpha\beta}; \alpha, \beta = (x, y, z, w)\}$, where S_α denotes inversion of r_α and $P_{\alpha\beta}$ permutation of r_α and r_β. There is, however, an additional symmetry. To explain it we use geometrical rather than group theory arguments. Inspection of Table I shows that all lattice points are located on parallel three-dimensional hyperplanes,

$$r_x + r_y + r_z + r_w = 2M \qquad (M \in \mathbb{Z}) \tag{2.1}$$

or equivalently

$$\boldsymbol{\theta} \cdot \mathbf{r} = M, \qquad \boldsymbol{\theta} = \tfrac{1}{2}(1, 1, 1, 1) \tag{2.2}$$

and form the *even* sublattice of the four-dimensional cubic lattice. The plane $\boldsymbol{\theta} \cdot \mathbf{r} = 0$ is a mirror plane. The reflected point $\mathbf{r}'$ is obtained by reflecting the component $\mathbf{r}_\perp = \boldsymbol{\theta}(\boldsymbol{\theta} \cdot \mathbf{r})$ of $\mathbf{r}$ perpendicular to the mirror, i.e.,

$$\mathbf{r}' \equiv S(\boldsymbol{\theta})\mathbf{r} = \mathbf{r} - 2\mathbf{r}_\perp = \mathbf{r} - 2\boldsymbol{\theta}\boldsymbol{\theta} \cdot \mathbf{r} \tag{2.3}$$

The reflection symmetry $S(\boldsymbol{\theta})$ leaves the set of lattice points invariant. Of course any linear combination of Cartesian components r_α ($\alpha = x, y, z, t$) with coefficients $a_\alpha = \pm 1$ satisfies $\sum_\alpha a_\alpha r_\alpha = 2M$. Therefore the first eight

Table I. Direct $\{\mathbf{c}_i\}$ and Reciprocal $\{\boldsymbol{\theta}_j\}$ Lattice Vectors $\{i, j = 1, 2,..., 24\}$

$\mathbf{c}_i$	$\boldsymbol{\theta}_j$	
$(\pm 1, \pm 1, 0, 0)$	$\pm\frac{1}{2}(1, 1, 1, 1)$	$\pm\frac{1}{2}(1, 1, -1, 1)$
$(\pm 1, 0, \pm 1, 0)$	$\pm\frac{1}{2}(1, 1, -1, -1)$	$\pm\frac{1}{2}(1, 1, 1, -1)$
$(\pm 1, 0, 0, \pm 1)$	$\pm\frac{1}{2}(1, -1, -1, 1)$	$\pm(1, 0, 0, 0)$
$(0, \pm 1, \pm 1, 0)$	$\pm\frac{1}{2}(1, -1, 1, -1)$	$\pm(0, 1, 0, 0)$
$(0, \pm 1, 0, \pm 1)$	$\pm\frac{1}{2}(-1, 1, 1, 1)$	$\pm(0, 0, 1, 0)$
$(0, 0, \pm 1, \pm 1)$	$\pm\frac{1}{2}(1, -1, 1, 1)$	$\pm(0, 0, 0, 1)$

$\hat{\mathbf{c}}_i \cdot \hat{\mathbf{c}}_j = \{0, \pm\frac{1}{2}, \pm 1\} = \boldsymbol{\theta}_i \cdot \boldsymbol{\theta}_j$

$\mathbf{c}_i \cdot \boldsymbol{\theta}_j = 0, \pm 1; \quad \hat{\mathbf{c}}_i \cdot \boldsymbol{\theta}_j = 0, \pm 1/\sqrt{2}$

entries $\boldsymbol{\theta}_j$ in Table I specify unit normal vectors of symmetry planes and corresponding symmetry operations $S(\boldsymbol{\theta}_j)$ that leave the FCHC lattice invariant. The symmetries S_α and $P_{\alpha\beta}$ guarantee the equivalence of these mirror planes. Furthermore, also the reflected vectors $\boldsymbol{\theta}_l' = S(\boldsymbol{\theta}_j)\,\boldsymbol{\theta}_l$ give new normal vectors of equivalent symmetry planes. By choosing $\boldsymbol{\theta}_j$ from the first group of four entries in Table I and $\boldsymbol{\theta}_l$ from the second (so that $\boldsymbol{\theta}_j \cdot \boldsymbol{\theta}_l = \pm 1/2$), one verifies that $\boldsymbol{\theta}_l'$ is one of the basis vectors $(\pm 1, 0, 0, 0)$, etc., in the third group. Therefore the planes $r_\alpha = M$ ($M = 0, \pm 1, \ldots$; $\alpha = x, y, z, w$) with sites restricted to the even sublattice belong to the set of 12 equivalent symmetry planes $\boldsymbol{\theta}_j \cdot \mathbf{r} = \pm M$ with $\boldsymbol{\theta}_j$ listed in Table I. The 24 unit vectors $\boldsymbol{\theta}_j$ are the *reciprocal* lattice vectors, corresponding to the 24 direct lattice vectors $\mathbf{c}_i$, and satisfy $\mathbf{c}_i \cdot \boldsymbol{\theta}_j = 0, \pm 1$, or $\mathbf{c}_i \cdot \hat{\boldsymbol{\theta}}_j = 0, \pm 1/\sqrt{2}$, where $\hat{\mathbf{a}} = \mathbf{a}/|\mathbf{a}|$ is a unit vector.

2.2. Stueckelberg Condition

There exist several FCHC lattice gases with 24 moving particles and with from zero up to seven rest particles.[1,2,18,19,29,27,28] The dynamics consists of collisions followed by propagation. The interactions are impulsive, as in hard-sphere systems. The particles are pointlike and possess only kinetic energy and unit mass.

The FCHC collision rules refer to a single node, and conserve the number of particles and the total momentum per node. In a single-speed model without rest particles ($b = 24$) energy and number conservation are the same. The collision rules are specified in terms of a $2^b \times 2^b$ transition matrix $A_{ss'}$ from a precollision or in-state $s(\mathbf{r}) = \{s_i(\mathbf{r});\ i = 1, 2, \ldots, b\}$ at node $\mathbf{r}$ to a postcollision or out-state $s'(\mathbf{r}) = \{s_i'(\mathbf{r});\ i = 1, 2, \ldots, b\}$ at the same node $\mathbf{r}$. The occupation numbers $s_i(\mathbf{r})$ are Boolean variables that take the values 0 or 1 if the velocity state $\{\mathbf{r}, \mathbf{c}_i\}$ is respectively empty or occupied. The matrix is normalized per row,

$$\sum_{s'} A_{ss'} = 1 \tag{2.4}$$

If collision rules are deterministic,[2] then all $A_{ss'}$ take integer values 0 or 1. Stochastic collision rules, as in refs. 18, 19, and 27, provide more flexibility ($0 \leqslant A_{ss'} \leqslant 1$). This is especially useful for the design of fully isotropic collision rules, which must obey $A_{ss'} = A_{P(s)\,P(s')}$ for any lattice symmetry P.

Some one-, two-, and three-dimensional lattice gases in the literature have a transition matrix that satisfies the detailed balance condition[29]

$$A_{s's} = A_{ss'} \tag{2.5}$$

In the majority of the unbiased FCHC models, however, A satisfies the less restrictive Stueckelberg condition,[9]

$$\sum_s A_{ss'} = 1, \qquad \forall s' \tag{2.6}$$

which has been called semi-detailed balance (SDB) in the context of lattice gases.[5] Note that (2.5) implies (2.6), and that deterministic SDB models have invertible dynamics.

The Stueckelberg condition ensures the existence of a universal factorized equilibrium state, both for the deterministic and the stochastic models, but it also restricts the degrees of freedom in fine tuning the collision rules. For that reason, several authors have constructed biased FCHC models without semi-detailed balance (NSDB), which optimize the Reynolds number. Thereby it is assumed that a factorized equilibrium state does exist for these models.[1,2,18,27]

2.3. The Somers–Rem Model

All graphical illustrations shown in this paper have been calculated using the Somers–Rem model.[18,3] This model does not involve rest particles ($b = 24$). The collision rules are stochastic and fully isotropic with respect to the group of lattice symmetries. In order to optimize the Reynolds efficiency per lattice unit, $Re_* = gc_s/\nu$, the Stueckelberg condition has been violated.

Collision rules have been selected that minimize the viscosity ν and maximize the non-Galilean factor g (the rate of convection), subject to the constraints of conservation of particle number, local momentum, and isotropy. Minimization of the viscosity involves minimization of[1,29]

$$\sum_{s,s' \in [N,\mathbf{P}]} A_{ss'} \sum_{\alpha,\beta} \sum_i s_i c_{i\alpha} c_{i\beta} \sum_j s'_j c_{j\alpha} c_{j\beta} \tag{2.7}$$

for each packet $[N, \mathbf{P}]$ of states with equal particle number N and total momentum $\mathbf{P}$. For many packets, the $A_{ss'}$ matrix is not uniquely specifiec by this optimization criterion and the given constraints. The remaining degrees of freedom are used to maximize the non-Galilean factor g by maximizing[18]

$$\sum_{s,s' \in [N,\mathbf{P}]} A_{ss'} \sum_i s'_i (\mathbf{c}_i \cdot \mathbf{P})^2 \tag{2.8}$$

for each packet $[N, \mathbf{P}]$.

The minimization of (2.7) is invariant under particle–hole duality $s_i \to 1 - s_i$, $s'_i \to 1 - s'_i$. As Eq. (2.7) is used as the primary optimization

criterion, the viscosity of the model will be symmetric around $\rho = 12$. The secondary criterion (2.8) tends to concentrate the particles at velocity directions that are parallel or antiparallel with the macroscopic flow direction. If sufficient degrees of freedom are available, the outcome of this optimization procedure will not exhibit particle–hole duality. From the numerical data of Fig. 1 it has indeed been verified that the eigenvalue λ (which is associated with the kinematic viscosity) is symmetric around $\rho = 12$, and that the eigenvalues ξ and τ are not symmetric, indicating that the collision rules do not exhibit particle–hole duality.

The Stueckelberg condition specifies that if all states in a packet $[N, \mathbf{P}]$ have an equal probability of occurrence as precollision state, then these states are also equally probable as after-collision state. An H-theorem[5] proves convergence toward a universal equilibrium state with a uniform probability distribution within each $[N, \mathbf{P}]$ packet. Hence, if the Stueckelberg condition holds, criterion (2.8) will not depend on the collision rules, and the g-factor will be universal: $2(24-2\rho)/3(24-\rho)$.

The implementation of the model involves an algorithm which reduces the full state space of 2^{24} entries into a set of 106,496 representative states, for which optimized collision rules are stored in a table that fits in the memory of modest computer equipment. Given a precollision state s, the reduction algorithm is capable of determining a suitable lattice isometry P_s, which transforms s into a unique representative state s_r for which the after-collision state s'_r is known from the table. The inverse lattice isometry is then used to compute the actual after-collision state $s' = P_s^{-1}(s'_r)$. Full isotropy of the collision operator is established by first applying a random isometry on the precollision state s and afterward its inverse on the postcollision state s'. The technical details of this algorithm can be found in ref. 3.

2.4. Physical and Spurious Invariants

As the collisions conserve the number of particles and momentum per node, the total number of particles $N = \sum_{r,i} s_i(\mathbf{r}, t)$ and total momentum $\mathbf{P} = \sum_{r,i} \mathbf{c}_i s_i(\mathbf{r}, t)$ in the system are conserved. At the macroscopic level the conservation laws for number and momentum density lead to the nonlinear Navier–Stokes equations of fluid dynamics. However, there are additional spurious invariants, as first discovered by Zanetti[23] for two-dimensional triangular lattice gases, referred to as staggered momenta. His arguments can be extended to FCHC lattice gases, as shown below.

Take any of the 12 equivalent three-dimensional mirror (hyper) planes $\boldsymbol{\theta} \cdot \mathbf{r} = M$, where the normal vector $\boldsymbol{\theta}$ is a reciprocal lattice vector. For a given $\boldsymbol{\theta}$ the lattice can be divided into an even $(+)$-sublattice (M is even)

and an odd $(-)$-sublattice (M is odd). Consider the total $\boldsymbol{\theta}$-momentum $P_{\theta}^{(+)}(t) = \sum_{r \in (+)} \sum_i \boldsymbol{\theta} \cdot \mathbf{c}_i s_i(\mathbf{r}, t)$ on the $(+)$-sublattice at time t. All particles with velocities in the hyperplane satisfy $\boldsymbol{\theta} \cdot \mathbf{c}_i = 0$ and do not contribute to $P_{\theta}^{(+)}(t)$. All particles with a nonvanishing component parallel to $\boldsymbol{\theta}$ satisfy $\boldsymbol{\theta} \cdot \mathbf{c}_i = \pm 1$ (see Table I), and will propagate at time $t+1$ to the nearest-neighbor planes belonging to the $(-)$-sublattice. Consequently $P_{\theta}^{(+)}(t) = P_{\theta}^{(-)}(t+1)$ and vice versa, and

$$H_{\theta} = (-1)^t [P_{\theta}^{(+)}(t) - P_{\theta}^{(-)}(t)] = \sum_{r,i} (-1)^{t+\theta \cdot r} \boldsymbol{\theta} \cdot \mathbf{c}_i s_i(\mathbf{r}, t) \tag{2.9}$$

is a constant of the motion, referred to as the staggered momentum. There are 12 similar mirror planes, and therefore also 12 conserved staggered momenta in FCHC models, specified by the reciprocal lattice vectors $\boldsymbol{\theta}_j$ listed in Table I. Obviously, inclusion of rest particles does not destroy these invariants, because they do not contribute to (2.9).

Knowledge of the existence and an understanding of the properties of these 12 additional locally conserved densities and corresponding transport coefficients is paramount for the validation of LGCA as tools to study the equations of fluid dynamics.

At the macroscopic level the staggered momentum densities give rise to 12 additional hydrodynamic equations that couple in a nonlinear fashion to the Navier–Stokes equations for the lattice gas fluids.[24,23] In the unphysical macroscopic equations new transport coefficients enter, called staggered diffusivities, which are calculated in Section 4.3. The spurious effects of the spurious slow variables should be suppressed as much as possible in LGCA simulations by preparing initial distributions with very small values of H_{θ}.

3. KINETIC THEORY

3.1. Mean Field Theory

In the present paper lattice gases are only described in mean field or Boltzmann approximation. Analytic results for FCHC models beyond mean field theory barely exist.[25,27,28,30]

The basic quantities in these theories are the distribution functions $f_i(\mathbf{r}, t) \equiv \langle s_i(\mathbf{r}) \rangle_{\text{ne}}$, where the occupation number $s_i(\mathbf{r})$ of the state $\{\mathbf{r}, \mathbf{c}_i\}$ is averaged over a nonequilibrium ensemble. Its time evolution is given by the nonlinear Boltzmann equation,

$$f_i(\mathbf{r} + \mathbf{c}_i, t+1) - f_i(\mathbf{r}, t) = \mathcal{J}_i(f(\mathbf{r}, t)) \tag{3.1}$$

This equation expresses the evolution of the distribution function subject to propagation and collisions $\mathscr{I}_i(f)$. The collision term $\mathscr{I}_i(f)$ can be expressed in terms of the collision matrix as[5]

$$\mathscr{I}_i(f) = \sum_{s,s'} (s_i' - s_i)\, A_{ss'} \prod_{j=1}^{b} f_j^{s_j}(1-f_j)^{1-s_j} \tag{3.2}$$

Due to mass and momentum conservation, $\mathscr{I}_i$ satisfies

$$\sum_i \mathscr{I}_i(f) = 0; \qquad \sum_i c_{i\alpha}\mathscr{I}_i(f) = 0 \tag{3.3}$$

where $\{1, c_\alpha; \alpha = x, y, z, w\}$ are collisional invariants. In this paper we follow the convention that all sums over $i, j, \ldots$ run over all velocity channels. Here $\{i = 1, 2, \ldots, b = 24\}$. In Appendix A the extension to rest particles is given.

If the transition matrix satisfies the Stueckelberg condition, one can prove that the H-function $H(t) = \sum_{\mathbf{r},i} f_i(\mathbf{r}, t) \ln f_i(\mathbf{r}, t)$ decreases monotonically to its equilibrium value. Furthermore, there exists a stable, unique, spatially uniform equilibrium state, and transport coefficients are positive.

In case the Stueckelberg condition (2.6) is not satisfied, an H-theorem does not exist, and existence of and convergence to a stable uniform and stationary equilibrium state cannot be guaranteed. However, if a uniform and stationary (not necessarily stable) solution $f_i(\mathbf{r}, \infty) = f$ of the lattice Boltzmann equation (3.1) exists for a 24-bit lattice gas at rest (vanishing total momentum), it is given by $f = \rho/24$ due to lattice symmetries.

3.2. Linearized Boltzmann Equation

To study the stability of the stationary solution $f = \rho/24$ of the 24-bit lattice gas one can linearize the lattice Boltzmann equation (3.1) around f and study its eigenvalues, which are related to the transport coefficients of the lattice gas.

These arguments are the motivation to study the linearized Boltzmann equation obtained by substituting $f_i(\mathbf{r}, t) = f + \delta f_i(\mathbf{r}, t)$ in (3.1) and keeping only terms linear in δf, i.e.,

$$\delta f_i(\mathbf{r} + \mathbf{c}_i, t+1) = \delta f_i(\mathbf{r}, t) + \sum_j \Omega_{ij}\delta f_j(\mathbf{r}, t) \tag{3.4}$$

where the stationarity relation $\mathscr{I}_i(f) = 0$ has been used. Its explicit form is derived in Appendix A. The complicated optimalization techniques for constructing collision rules in the different FCHC lattice gases[2,18,19] do not allow a simple analytic specification of the $2^{24} \times 2^{24}$ transition matrix $A_{ss'}$.

Nevertheless the 24×24 collision matrix Ω has for general collision rules a simple structure because of conservation laws, lattice symmetries, and the restriction to a single-speed model. It is symmetric and has only three independent matrix elements (see Appendix A). Its eigenvectors and eigenvalues are defined as

$$\Omega u_n = -\omega_n u_n \tag{3.5}$$

where $u_n(\mathbf{c})$ is a 24-vector with components $\{u_n(\mathbf{c}_i);\ i = 1, 2, \ldots, 24\}$. Inner products are denoted by

$$\langle a \mid b \rangle = \sum_i a_i b_i \tag{3.6}$$

The 24 eigenvectors $u_n(\mathbf{c})$ are completely determined by lattice symmetries, and given as tensor polynomials, with corresponding eigenvalues:

$$\begin{aligned}
u_n(\mathbf{c}) &= 1,\ c_\alpha && (\omega_n = 0,\ \mu_n = 5,\ \alpha = x, y, z, w) \\
u_{\alpha\beta}(\mathbf{c}) &= c_\alpha c_\beta - \tfrac{1}{2}\delta_{\alpha\beta} && (\omega_n = \lambda,\ \mu_n = 9) \\
u_{\alpha\beta\beta}(\mathbf{c}) &= c_\alpha (c_\beta^2 - \tfrac{1}{3}) && (\omega_n = \xi,\ \mu_n = 8,\ \alpha \neq \beta) \\
u_{\alpha\alpha\beta\beta}(\mathbf{c}) &= (c_\alpha^2 - \tfrac{1}{2})(c_\beta^2 - \tfrac{1}{2}) + \tfrac{1}{12} && (\omega_n = \tau,\ \mu_n = 2,\ \alpha \neq \beta)
\end{aligned} \tag{3.7}$$

where μ_n is the multiplicity of eigenvalue ω_n. The eigenvectors u_n corresponding to the same eigenvalue ω_n span a μ_n-dimensional space,[5] but are not yet orthogonalized.

The nonvanishing eigenvalues λ, ξ, τ can be expressed in the matrix elements Ω_{ij}, which are evaluated numerically using the formulas (A.2) in Appendix A. Figure 1 shows their numerical values as a function of ρ for the Somers–Rem collision rules. As we shall see, the eigenvalue λ determines the kinematic viscosity. In the lattice gas literature the eigenfunctions with $\omega_n = \xi$ or τ are frequently referred to as "ghosts." The eigenvalue $\lambda(\rho) = \lambda(24 - \rho)$ is symmetric, as in self-dual models. This is a consequence of the optimalized collision rules. Closer inspection of Fig. 1 reveals that the eigenvalues $\xi(\rho)$ and $\tau(\rho)$ do not posses this symmetry, because the Somers–Rem model is not self-dual.

[5] The equality of the eigenvalues corresponding to u_{xx} and u_{xy} in (3.7) is a direct consequence of the extra symmetry (2.3) of the FCHC lattice. This extra equality is also the essential ingredient for proving that the viscosity tensor in FCHC models simplifies from cubic to isotropic.

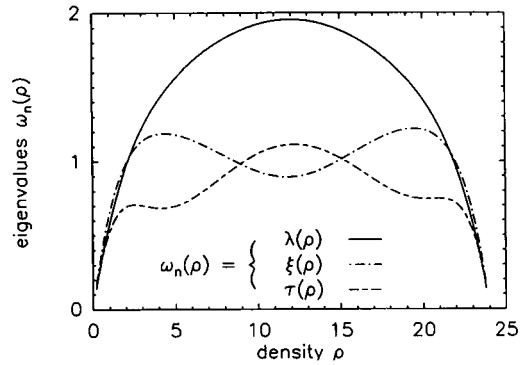

Fig. 1. Eigenvalues λ, ξ, τ of the linear collision operator Ω for the NSDB model of Somers and Rem as a function of the density ρ, where $\lambda(\rho)$ is symmetric around $\rho = 12$, but ξ and τ are not.

4. RELAXATION SPECTRUM

4.1. Eigenvalue Problem

Of most physical interest are the hydrodynamic or slow modes—here shear and sound modes—because their decay rates are given by transport coefficients.[31] In fact the calculation of the eigenvalues or decay rates is an attractive and simple alternative to the Chapman–Enskog method[32] or the multi-time-scale formalisms[5] to calculate the transport coefficients in the FCHC models. We follow this method in the present paper.

After this motivation we turn to the eigenvalue problem. As Ω is translationally invariant, it is convenient to perform a Fourier analysis and substitute

$$\delta f_i(\mathbf{r}, t) = e^{i\mathbf{k}\cdot\mathbf{r} + z(k)t}\psi(\mathbf{k}, \mathbf{c}_i) \tag{4.1}$$

into the kinetic equation (3.4), which reduces to the eigenvalue equation

$$\mathscr{S}^{-1}(1 + \Omega)\,\psi_n = \Lambda_n \psi_n \tag{4.2}$$

where ψ_n is a b-vector with components $\psi_{n_i} = \psi_n(\mathbf{k}, \mathbf{c}_i)$. The propagation operator $\mathscr{S}(\mathbf{k}) = \exp(i\mathbf{k}\cdot\mathbf{c})$ is a diagonal matrix with $\mathscr{S}_{ij}(\mathbf{k}) = \delta_{ij}\exp(i\mathbf{k}\cdot\mathbf{c}_i)$. Eigenvectors and eigenvalues are denoted by ψ_n and $\Lambda_n(\mathbf{k}) = \exp[z_n(\mathbf{k})]$, respectively. The matrices $\mathscr{S}$ and Ω are symmetric, but $\mathscr{S}^{-1}\Omega$ is not. Left and right eigenfunctions $\tilde{\psi}_n$ and ψ_n are therefore different[21,33] and form a biorthogonal set satisfying $\langle \tilde{\psi}_n \mid \psi_m \rangle = \mathscr{N}_n \delta_{nm}$, where $\mathscr{N}_n$ is a normalization constant. The wavevector $\mathbf{k}$ belongs to the

reciprocal lattice $\mathscr{L}^*$ of the FCHC lattice with sites $\mathbf{Q} = 2\pi \sum_l N_l \boldsymbol{\theta}_l$, where N_l are integers and $\{\boldsymbol{\theta}_l\}$ form a set of four independent unit vectors taken from Table I. The vector $\mathbf{k}$ can be restricted to the first Brillouin zone because

$$z_n(\mathbf{k}) = z_n(\mathbf{k} + \mathbf{Q}) \tag{4.3}$$

is a periodic function. The real part of the eigenvalue determines its stability. If $\mathrm{Re}\, z_n(\mathbf{k}) < 0$, the mode n is stable and decays. If $\mathrm{Re}\, z_n(\mathbf{k}) > 0$, in some range of $\mathbf{k}$-values, spontaneous fluctuations of that wavelength will grow, and the mode is unstable. If the imaginary part $\mathrm{Im}\, z_n(\mathbf{k}) \equiv c_s(\mathbf{k})k$ is nonvanishing, the mode is propagating with a phase velocity $c_s(\mathbf{k})$ (where $k = |\mathbf{k}|$). The long-wavelength excitations ($\mathbf{k} \to 0$) are soft (slowly decaying) *hydrodynamic* modes with $z_n(\mathbf{k} = 0) = 0$, or hard (rapidly decaying) *kinetic* modes with $z_n(\mathbf{k} = 0) \neq 0$.

The soft modes consist of two propagating sound modes ψ_σ with $\sigma = \pm$, and three shear or transverse momentum modes $\psi_{\perp\alpha}$ with $\alpha = 1, 2, 3$, referring to three independent transverse directions $\mathbf{e}_\alpha(\mathbf{k})$, perpendicular to $\hat{\mathbf{k}}$. In the limit of small $\mathbf{k}$ the eigenvalues are given by the hydrodynamic dispersion relations[31]

$$\begin{aligned} z_\sigma(\mathbf{k}) &= -i\sigma c_s k - \Gamma k^2 \qquad (\sigma = \pm) \\ z_{\perp\alpha}(\mathbf{k}) &= -\nu k^2 \qquad\qquad (\alpha = 1, 2, 3) \end{aligned} \tag{4.4}$$

where ν is identified as the kinematic viscosity and Γ as the sound damping constant, with $k = |\mathbf{k}|$. Therefore a perturbation calculation of $z_n(\mathbf{k})$ for small $\mathbf{k}$ yields the transport coefficients, as will be shown in the next subsection.

4.2. Perturbation Theory

The eigenvalues $z_n(\mathbf{k})$ of the two-dimensional lattice Boltzmann equation have been studied in the literature,[22,34] also in systems with unstable modes.[15,35] Here the same method is applied to the pseudo-three-dimensional FCHC models, and we briefly summarize the results.

We first consider the hydrodynamic modes and eigenvalues following the method explained in ref. 22. In the limit of small $\mathbf{k}$ it is convenient to write the eigenvalue equation (4.2) as

$$[e^{z_n(k) + ik\cdot c} - 1 - \Omega]\, \psi_n = 0 \tag{4.5}$$

and to expand eigenvalues, $z_n = z_n^{(0)} + ikz_n^{(1)} + \cdots$, and eigenfunctions, $\psi_n = \psi_n^{(0)} + ik\psi_n^{(1)} + \cdots$, in powers of ik, where $z_n^{(0)} = 0$ for hydrodynamic

modes. The resulting equations can be solved order by order, and one finds for the eigenvalues of shear modes ($n = \perp\alpha$; $\alpha = 1, 2, 3$) and sound modes ($n = \sigma$; $\sigma = \pm$) to order (ik)

$$z_{\perp\alpha}^{(1)} = 0, \qquad z_{\sigma}^{(1)} = -\sigma c_s = -\sigma/\sqrt{2} \tag{4.6}$$

and to order $(ik)^2$

$$\begin{aligned} z_{\perp\alpha}^{(2)} \equiv \nu &= -\langle c_l c_{\perp\alpha} | \frac{1}{\Omega} + \frac{1}{2} | c_l c_{\perp\alpha} \rangle / \langle c_{\perp\alpha} | c_{\perp\alpha} \rangle \\ z_{\sigma}^{(2)} \equiv \Gamma &= -\frac{1}{2} \langle c_l^2 - c_s^2 | \frac{1}{\Omega} + \frac{1}{2} | c_l^2 - c_s^2 \rangle / \langle c_l | c_l \rangle \end{aligned} \tag{4.7}$$

where $c_l = \hat{\mathbf{k}} \cdot \mathbf{c}$ and $c_{\perp\alpha} = \mathbf{e}_\alpha(\mathbf{k}) \cdot \mathbf{c}$ are longitudinal and transverse components of $\mathbf{c}$ and $\{\hat{\mathbf{k}}, \mathbf{e}_\alpha(\mathbf{k}); \alpha = 1, 2, 3\}$ is a complete set of orthogonal unit vectors.

The same expressions have been obtained before for two-dimensional LGCA.[36] In this manner we have derived expressions for the transport coefficients in mean field approximation, where Ω^{-1} is the (quasi) inverse of Ω in the orthogonal complement of the nullspace (spanned by the collisional invariants). It should be noted that these formulas (4.7) are valid for all isotropic d-dimensional LGCA. In Appendix B this result is extended to the bulk viscosity by including an arbitrary number of rest particles. The Chapman–Enskog results for transport coefficients in continuous gases have essentially the same form as (4.7), with $\Omega^{-1} + 1/2$ replaced by Ω^{-1}. Of course, there Ω is an integral operator and the definition of inner products includes a Maxwell–Boltzmann factor as weight factor.[32]

For FCHC models without rest particles these expressions can be calculated directly in tems of a single eigenvalue by observing that both $c_l c_{\perp\alpha}$ and $c_l^2 - c_s^2$ with $c_s^2 = 1/2$ are linear combinations of eigenfunctions $u_{\alpha\beta}(\mathbf{c})$ in (3.7) with eigenvalue λ. A simple calculation yields then

$$\nu = \frac{1}{3}\left(\frac{1}{\lambda} - \frac{1}{2}\right); \qquad \Gamma = \frac{3}{4}\nu \tag{4.8}$$

In general the expressions in (4.7) depend on the direction of $\mathbf{k}$. This is for instance the case in lattices with only cubic symmetry. However, the extra symmetry (2.3) of the FCHC lattice makes the eigenfunctions $c_x c_y$ and $c_x^2 - 1/2$ *degenerate*, and guarantees the isotropy of the viscosity tensor in FCHC models.

The viscosity tensor contains a kinematic viscosity ν and a bulk viscosity ζ. In single-speed models like the FCHC models considered above, ζ is vanishing. However, in models with one or more rest particles,

ζ is nonvanishing. In Appendix B we show that the sound damping constant for such systems is given by a form very similar to (4.7). For FCHC models this can be written as $\Gamma = \frac{3}{4}\nu + \frac{1}{2}\zeta$, where the bulk viscosity is given by

$$\zeta = \left(\frac{1}{2} - c_s^2\right)\left(\frac{1}{\varpi_2} - \frac{1}{2}\right) \tag{4.9}$$

The eigenvalue ϖ_2, calculated in (A.6) of Appendix A, depends only on matrix elements of Ω connecting rest particles with moving particles.

4.3. Staggered Momentum Modes

The existence of the spurious conservation law in (2.9) for a given $\boldsymbol{\theta}$ implies the existence of a slow mode, the staggered momentum mode, for $\mathbf{k}$ close to $\pi\boldsymbol{\theta}$, as discussed in Appendix C. Its amplitude decays as

$$\exp[z_\theta(\mathbf{k})t] = (-1)^t \exp[-D_\theta(\hat{\mathbf{k}})\,|\mathbf{k} - \pi\boldsymbol{\theta}|^2\, t]$$

as shown in ref. 36. The analysis and explicit calculation of the staggered diffusivities for FCHC models are new, and apply to all FCHC models with or without rest particles.

For the staggered diffusivity we obtain an expression which depends on the angle between $\hat{\mathbf{k}}$ and $\hat{\boldsymbol{\theta}}$, i.e.,

$$\begin{aligned} D_\theta(\hat{\mathbf{k}}) &= -\langle c_\theta c_l | \frac{1}{\Omega + \Delta(c_\theta)} + \frac{1}{2} | c_\theta c_l \rangle / \langle c_\theta \mid c_\theta \rangle \\ \Delta(c_\theta) &= 1 + (-1)^{\theta \cdot c} = 2(1 - c_\theta^2) \end{aligned} \tag{4.10}$$

with $c_\theta = \boldsymbol{\theta} \cdot \mathbf{c}$ and $c_l = \hat{\mathbf{k}} \cdot \mathbf{c}$. Explicit calculation in Appendix C yields an anisotropic diffusivity

$$\begin{aligned} D_\theta(\hat{\mathbf{k}}) &= D_{\|} \cos^2 \chi + D_\perp \sin^2 \chi \\ &= 6\nu \cos^2 \chi + \nu \sin^2 \chi \end{aligned} \tag{4.11}$$

with $\cos \chi = \hat{\boldsymbol{\theta}} \cdot \hat{\mathbf{k}}$.

As $z_\theta(\mathbf{k}) = z_\theta(\mathbf{k} + \mathbf{Q})$ on account of (4.3), there is a spurious soft mode at all points $\mathbf{Q} + \pi\boldsymbol{\theta}$, where $\mathbf{Q}$ is a site of the reciprocal lattice $\mathscr{L}^*$ (see Section 4.1) and $\boldsymbol{\theta}$ any of the $\boldsymbol{\theta}$-vectors in Table I. For instance, in case $\mathbf{k} \| (1, 0, 0, 0)$ there exists a slow staggered mode at $\mathbf{k}_0 = \pi(1, 0, 0, 0) = \pi\boldsymbol{\theta}$ with $\cos \chi = \hat{\boldsymbol{\theta}} \cdot \hat{\mathbf{k}} = 1$. The decay rate of the mode is

$$z_\theta(\mathbf{k}) = \pi i - 6\nu(k - \pi)^2 \tag{4.12}$$

For $\mathbf{k} \parallel (1, 1, 1, 0)$ there is a staggered mode at $\mathbf{k}_1 = \pi(1, 1, 1, 0) = \mathbf{Q} - \pi\boldsymbol{\theta}$, characterized by $\boldsymbol{\theta} = (0, 0, 0, 1)$ with $\cos\chi = \hat{\mathbf{k}} \cdot \hat{\boldsymbol{\theta}} = 0$. The decay rate is

$$z_\theta(\mathbf{k}) = \pi i - v(k - \pi\sqrt{3})^2 \tag{4.13}$$

5. NUMERICAL RESULTS

The relevance of the information obtained by the numerical calculation of the eigenvalues of (4.5) is discussed extensively in refs. 22 and 34. Here we restrict ourselves to discussing some generic properties of FCHC spectra.

The numerical problem of finding the eigenvalues $\Lambda_n(\mathbf{k}) = \exp[z_n(\mathbf{k})]$ of (4.2) is relatively simple. It involves the calculation of the 24 roots of the secular determinant of the complex matrix in (4.2) as a function of wavenumber $\mathbf{k}$ and density $f = \rho/24$. The eigenvalues $z_n(\mathbf{k})$ are in general complex with $\mathrm{Im}\, z_n(\mathbf{k})$ defined modulo 2π. Figure 2 shows a typical eigen-

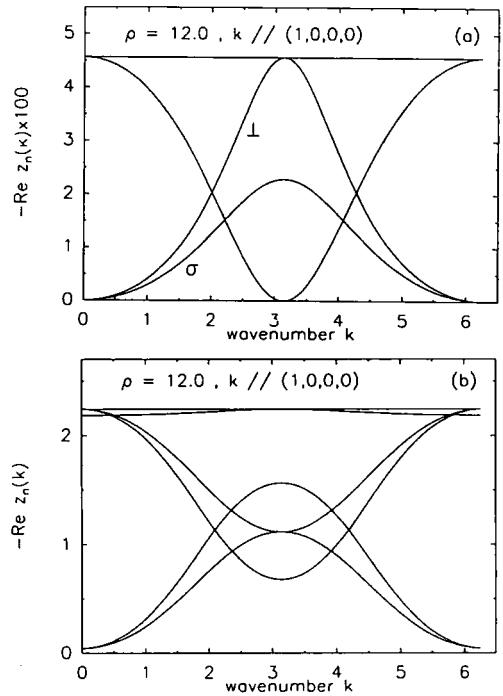

Fig. 2. Spectrum of $-\mathrm{Re}\, z_\mu(k)$ versus the wavevector k for the NSDB FCHC model. The density is $\rho = 12$, and $\mathbf{k}$ is parallel to $(1, 0, 0, 0)$. (a) The lower part of the spectra, where slow modes are seen at $k \simeq 0$ (hydrodynamic) and $k \simeq \pi$ (staggered). (b) Only kinetic modes.

value spectrum at density $\rho = 12$ for the real part of $z_n(\mathbf{k})$ with $\mathbf{k}$ parallel to a reciprocal lattice vector $\boldsymbol{\theta}_j$, as listed in Table I. Figures 2a and 2b show, respectively, the 9 smallest and 15 largest eigenvalues. The $\mathbf{k}$-period in a $\boldsymbol{\theta}$-direction is 2π. The plots indicate that all modes are linearly stable, i.e., $\mathrm{Re}\, z_n(\mathbf{k}) < 0$. This appears to be the case for all $\mathbf{k}$ and for all densities ρ.

Figure 2a shows *five soft hydrodynamic* modes with $\mathrm{Re}\, z_n(k)$ vanishing like $\mathcal{O}(k^2)$ as $\mathbf{k} \to 0$. Two of these modes are propagating sound modes with a nonvanishing $\mathrm{Im}\, z_n(\mathbf{k}) = \pm c_s(\underline{\mathbf{k}})k$. In the long-wavelength limit the speed of sound $c_s(\mathbf{k})$ approaches $1/\sqrt{2}$, independent of magnitude and direction of $\mathbf{k}$, as illustrated in Fig. 3. For long wavelengths with $2\pi/k > 8$ lattice units, the sound speed varies by less than 2% in the Somers–Rem model.

In Fig. 2 one further observes the purely diffusive shear mode (labeled $\perp$), which is threefold degenerate, and two propagating damped sound modes (labeled σ). According to (4.4), the long-wavelength limit of the real part of the hydrodynamic eigenvalues determines the (constant) transport coefficients ν and Γ. We also note that the damping constants of shear and sound modes are small compared to those of kinetic modes in a sufficiently large range of k values ($k \leqslant 1$ or $\lambda \gtrsim 6$), so that hydrodynamic and kinetic time scales are well separated. This range covers both classical hydrodynamics with constant transport coefficients as well as generalized hydrodynamics. The horizontal line in Fig. 2a at $\omega_n(k) = 4.6$ represents a constant eigenvalue.

In generalized hydrodynamics one considers a wavenumber-dependent kinematic viscosity $\nu(\mathbf{k}) = -z_{\perp\alpha}(\mathbf{k})/k^2$ and sound damping constant $\Gamma(\mathbf{k}) = -\mathrm{Re}\, z_\sigma(\mathbf{k})/k^2$. These functions are respectively shown in Fig. 4 and 5 for two different directions at density $\rho = 4$. Perhaps the most important

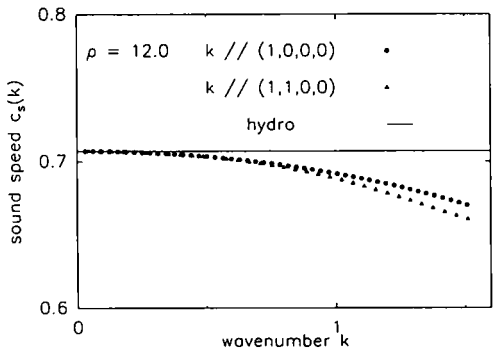

Fig. 3. Speed of sound $c_s(k)$ versus k for density $\rho = 12$. The solid line corresponds to the long-wave length result, $c_s = 1/\sqrt{2}$. Symbols refer to $\mathrm{Im}\, z_n(\mathbf{k})/k$ for $\mathbf{k}$ parallel to (1, 0, 0, 0) (dots) and $\mathbf{k}$ parallel to (1, 1, 0, 0) (triangles), obtained by numerically solving the eigenvalue spectrum.

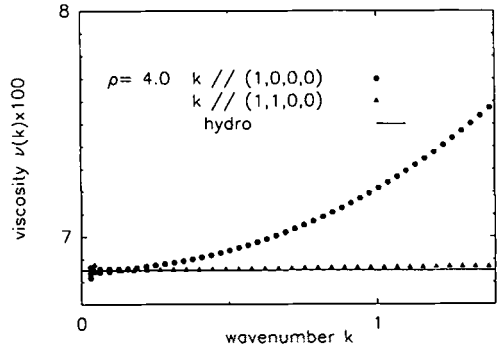

Fig. 4. Viscosity $\nu(k)$ versus k for density $\rho = 4$. The solid line is the hydrodynamic value given by Eq. (4.8). Symbols refer to the results obtained by numerical evaluation of the spectrum. These results practically coincide with the hydrodynamic value for **k** parallel to (1, 0, 0, 0) (circles). For **k** parallel to (1, 1, 0, 0) (triangles) the deviations are bigger.

observation to be inferred from Fig. 4 is that the damping constants $\nu(\mathbf{k})$ and $\Gamma(\mathbf{k})$ of the hydrodynamic modes are positive for *all* **k** values, so that the spatially uniform state is stable for the Somers–Rem FCHC lattice gas with NSDB collision rules. From the point of view of physical validation of FCHC lattice gases, this positivity is a point in favor of the Somers–Rem model, as compared to Hénon's NSDB FCHC-9 model,[2] where the kinematic viscosity is negative at small **k** values. Furthermore, as $\mathbf{k} \to 0$, viscosity and sound damping approach the constant values ν and $\Gamma = \frac{3}{4}\nu$, in agreement with (4.8), where λ is given in Fig. 1. We further note that near the *smallest* wavenumbers ($k \simeq 0.03$) the threefold degeneracy in Fig. 4

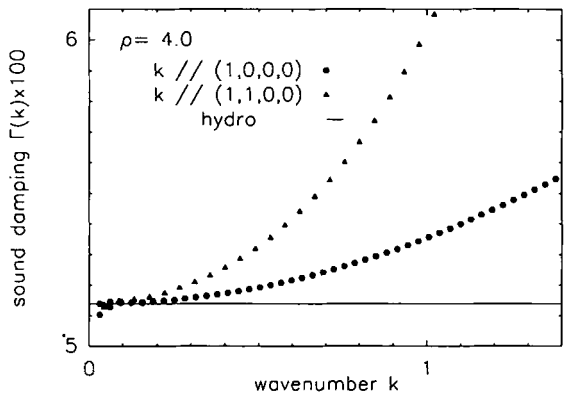

Fig. 5. The same as in Fig. 4, but for the sound damping constant $\Gamma(k)$. Here deviations between the hydrodynamic value and those obtained from the spectrum are more pronounced.

and the twofold one in Fig. 5 of the hydrodynamic eigenvalue $\mathrm{Re}\, z_n(\mathbf{k})/\mathbf{k}^2$ are lifted by numerical inaccuracy. The Somers–Rem FCHC lattice gas is well suited for simulating hydrodynamic equations, because classical hydrodynamics is observed for $k \leqslant 0.5$, where $\nu(k)$ and $\Gamma(k)$ deviate, respectively, by less than 2% and 4% from their long-wavelength limit. At finite $\mathbf{k}$ values the sound damping constant $\Gamma(\mathbf{k})$ differs from $\frac{3}{4} \times \nu(\mathbf{k})$. The viscosity increases at most 7% when k increases to 1.5. The sound damping constant increases much more rapidly. A similar $\mathbf{k}$ dependence of $\nu(\mathbf{k})$ and $\Gamma(\mathbf{k})$ is found at other densities. We have further noticed that the propagating sound modes may become diffusive and that, conversely, pairs of purely diffusive modes may become propagating.

There is also a clear signal of the existence of a spurious conservation law present in Fig. 2, namely an eigenvalue $z_n(\mathbf{k})$ *that vanishes at a finite* $\mathbf{k}$ *value.* This is one of the spurious staggered momentum modes discussed in Eq. (4.12) of Section 4.3. We have numerically verified that $\mathrm{Re}\, z_0(\mathbf{k})$ is indeed given by a quadratic form like (4.9) and (4.11) with staggered diffusivities given by $D_0 = D_\parallel = 6\nu$. According to (4.11), the staggered diffusivity is anisotropic. We have also verified numerically that for $\mathbf{k} \parallel (1, 1, 1, 0)$ the staggered diffusivity is given by $D_0 = D_\perp = \nu$, and that for $\mathbf{k} \parallel (1, 1, 0, 0)$ the staggered mode is absent, in agreement with the analytic result of Section 4.3.

One of the striking new features of all FCHC spectra, as compared to those of the more common triangular lattice gases,[22] is their high degree of degeneracy. Among a total of 24 eigenvalues, only four eigenvalues $\omega = \{0, \lambda, \xi, \tau\}$ are distinct at $\mathbf{k} = 0$. For finite $\mathbf{k}$ values the degeneracies are only partially lifted, depending on the $\mathbf{k}$ direction. For $\mathbf{k}$ parallel to $(1, 0, 0, 0)$, $(1, 1, 0, 0)$, and $(1, 1, 1, 0)$ there are only 10, 12, and 15 eigenvalues with distinct $\mathrm{Re}\, z_n(\mathbf{k})$. These numbers can be understood on the basis of the symmetries that leave the matrix $\mathscr{S}^{-1}(1 + \Omega)$ invariant. On the basis of these symmetries one can construct different sets of basis vectors $u_n(\mathbf{c})$ appropriate for the diagonalization of the matrix $\mathscr{S}^{-1}(1 + \Omega)$ for any $\mathbf{k}$ vector parallel or perpendicular to the lattice vectors. In fact many properties of the FCHC spectra can be explained in great detail,[22,37] but will not be discussed here any further.

6. SIMULATIONS

6.1. Velocity Correlations

As mentioned in the introduction, the equilibrium state of NSDB FCHC lattice gases is not the Gibbs state, because the equal-time velocity correlation function in equilibrium does not vanish, whereas it does vanish

in the Gibbs state.[10] Here we restrict ourselves to the observation of equal-time two-point correlations on the same node in equilibrium for the Somers–Rem model. They are defined as

$$C_{ij} \equiv C(\rho, \phi_{ij}) = \frac{\langle \delta s_i \, \delta s_j \rangle}{[\langle (\delta s_i)^2 \rangle \langle (\delta s_j)^2 \rangle]^{1/2}} = \frac{\langle s_i s_j \rangle - f^2}{f(1-f)} \tag{6.1}$$

where the averages are taken at a fixed time over the whole lattice and where $\delta s_i = s_i - f$, with $f = \rho/24$. As the equilibrium correlations $\langle s_i s_j \rangle$ possess all the FCHC symmetries, it depends only on the angle $\phi_{ij} = \arccos(\hat{\mathbf{c}}_i \cdot \hat{\mathbf{c}}_j)$ between the velocity directions. There are only five different values of ϕ_{ij} according to Table I.

To improve the statistics we average C_{ij} over all pairs with the same angle ϕ_{ij}.[6] In the FCHC lattice there are $\mathcal{N}(\pi/3) = \mathcal{N}(2\pi/3) = 96$ pairs with $\phi_{ij} = \pi/3$ and $2\pi/3$, respectively, $\mathcal{N}(\pi/2) = 72$ with $\phi_{ij} = \pi/2$, and $\mathcal{N}(\pi) = 12$ with $\phi_{ij} = \pi$, and of course $\mathcal{N}(0) = 24$. All simulations are performed on a quasi-three-dimensional system of $20 \times 20 \times 20 \times 2$ lattice units. In the initial state every velocity channel is occupied with equal probability $\rho/24$. For the unbiased FCHC model of ref. 19 we find indeed vanishing correlations. In simulating the biased FCHC model of ref. 18 we observe a rapid buildup of correlations within 50 time steps, which remain constant as time progresses (tested up to 10,000 time steps). Figures 6A–6D show the pre- and postcollision correlation functions on a single node for all four angles. For a definition of the postcollision correlations we refer to ref. 10.

Figure 6 shows the density-dependent pre- and postcollision correlations for all angles. As we can see, the precorrelation is systematically smaller than the postcorrelation (by factors of approximately 1.5 for $2\pi/2$ to 4 for $\pi/2$); this is to be expected, as the propagation step moves the particles to different nodes. This acts as a reshuffling, which partially destroys the velocity correlations.

The optimalization techniques used by Somers and Rem in constructing their collision tables have the tendency to produce output particles moving parallel or antiparallel to the local momentum density, and thus to each other. We therefore expect that the angle π gives a large, positive correlation, and $\pi/2$ gives a relatively large, but negative correlation. The angles $\pi/3$ and $2\pi/3$ show smaller correlations (in absolute value). This is also understandable in view of the argument above. In fact similar correlations are observed in all NSDB FCHC models. It has been noted by Hénon that the properties of the NSDB model FCHC-6 strongly resemble

[6] Hénon has pointed out to us that the correlations C_{ij} in a quasi-three-dimensional system are strongly anisotropic, and may differ by a factor of two depending on whether $\mathbf{c}_i$ and $\mathbf{c}_j$ have a component in the fourth dimension.[26]

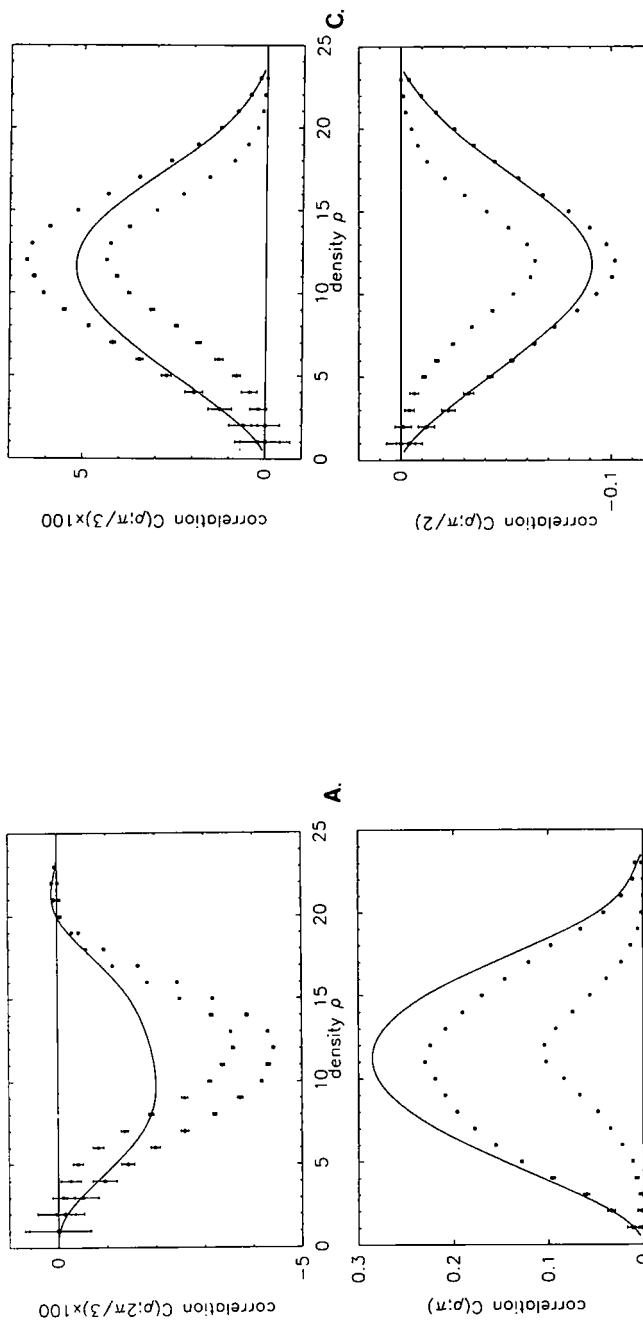

Fig. 6. Correlation functions $C(\rho, \phi_{ij})$ for different angles (A) $\phi_{ij} = \frac{2}{3}\pi$, (B) $\phi_{ij} = \pi$, (C) $\phi_{ij} = \frac{1}{3}\pi$, (D) $\phi_{ij} = \pi/2$ at density $\rho = 5.0$. The solid line is the mean field result of ref. 10 and symbols are simulation results. Squares are precollision correlations and circles are postcollision correlations. Note that the scale for palens (A) and (C) is 100 times bigger than that of (B) and (D).

the Somers–Rem model, and that the SDB model of Westland is similar to the FCHC-3 model.[26]

It is interesting to know how much correlation the collision table builds up starting from a fully factorized lattice state, i.e., with no correlations at all. This is shown by the solid lines in Fig. 6. They represent the theoretically predicted postcollision correlations that are built up through the biased collision rules in a single collision step, starting from a precollision state with a totally uncorrelated velocity distribution. How to compute these quantities from the transition matrix $A_{s's}$ is shown in ref. 10, to which we refer for details.

The mean field plots show qualitatively as well as quantitatively a reasonably good agreement with the simulation results. Only in the $C(\rho, 2\pi/3)$ plot is the relative deviation from simulation values substantial, for which we have no explanation. The comparison suggests a *quick* buildup of correlations during the collision step, whereas the reshuffling of particles during the propagation step destroys part of the correlations.

6.2. Speed of Sound

To measure the speed of sound and sound damping coefficient we follow the method of Dubrulle *et al.*[1] We set up a longitudinal wave $v_x(0) = v_{x0} \sin kx$ in the initial flow field $\mathbf{v}$. The system size is $60 \times 20 \times 20$ and we have chosen $k = 2\pi/60 \simeq 0.1$, well inside the region of classical hydrodynamics (see Fig. 3). The initial amplitude should satisfy $v_{x0} \ll c_s = 1/\sqrt{2}$, and is chosen such that $\mathcal{O}(v^2) \simeq \mathcal{O}(\nabla v)$. To linear order this wave will relax as a superposition of two sound modes

$$v_x(k, t) = v_{x0} \cos(c_s k t) \exp(-\Gamma k^2 t) \tag{6.2}$$

The initial amplitude was chosen as $v_{x0} = 0.05$. After a sufficiently long equilibration period of 100 time steps the speed of sound was measured by locating the zero crossings in (6.2) up to 800 time steps. For longer times the signal-to-noise ratio becomes too small. The measurements were done at an average density of $\rho = 5.0$ particles per node with the number of particles typically about 2.4×10^5, and the results were averaged over three runs.

Using this method, we obtained the following results for the speed of sound: $c_s = 0.707 \pm 0.002$ for the SDB FCHC model,[19] satisfying the Stueckelberg condition, and $c_s = 0.724 \pm 0.005$ for the NSDB FCHC lattice gas model of Somers and Rem. The statistical accuracy was insufficient to extract values for the damping coefficient Γ. In the absence of rest particles the prediction of kinetic theory for the speed of sound is $c_s =$

$1/\sqrt{2} \simeq 0.7071$, independent of the validity or violation of (semi)-detailed balance, at least for models without rest particles. In the presence of rest particles the speed of sound c_s does depend on the collision rules, as calculated explicitly in Appendix B. The measured value in the NSDB case without rest particles exceeds the theoretical value by about 3%. This is well outside the error bars. The discrepancy between the kinetic theory value and the measured value is caused by the equilibrium velocity correlations measured in the previous subsection.

The *linear response theory* of Ernst and Dufty [see ref. 17, Eq. (4.2)] gives an expression for the speed of sound, in which on-node correlations are kept, but off-node correlations are neglected, i.e.

$$c_s^2 = \frac{\langle g_x \mid g_x \rangle}{\langle \rho \mid \rho \rangle} = \frac{1}{d} \frac{\sum_{ij} \mathbf{c}_i \cdot \mathbf{c}_j \langle \delta s_i(\mathbf{r})\, \delta s_j(\mathbf{r}) \rangle}{\sum_{ij} \langle \delta s_i(\mathbf{r})\, \delta s_j(\mathbf{r}) \rangle} \tag{6.3}$$

where d is the spatial dimension ($d=4$ in the FCHC model). This expression contains the on-node velocity correlations for $i \neq j$, which are present in the NSDB FCHC equilibrium state, and are missing in the Boltzmann approximation $c_s = 1/\sqrt{2} \simeq 0.707$. On the other hand, in SDB FCHC models, where velocity correlation is absent, (6.3) reduces to the kinetic theory result, $c_s^2 = c_0^2/d = 1/2$ for FCHC models.

Furthermore, using the results of the previous subsection, we are able to evaluate (6.3) for our FCHC model, i.e.,

$$c_s^2 = \frac{1}{2} \frac{\sum_\phi \mathcal{N}(\phi) \cos\phi C(\rho, \phi)}{\sum_\phi \mathcal{N}(\phi)\, C(\rho, \phi)} \simeq 0.723 \tag{6.4}$$

where the summation runs over $\phi = 0$, $\pi/3$, $\pi/2$, $2\pi/3$, and π. The multiplicities are given in the previous subsection and the values $C(\rho, \phi)$ at $\rho = 5.0$ can be read off from Fig. 6.

The simulation value 0.724 ± 0.005 is in *good agreement* with the predictions of *linear response theory*, which takes on-node equilibrium velocity correlations into account, and *disagrees* with the prediction of the approximate *Boltzmann equation*. We further observe that the speed of sound measured by Dubrulle *et al.* in the deterministic NSDB FCHC-6 model is smaller than $1/\sqrt{2}$, although the model is reported[26] to resemble the stochastic NSDB Somers–Rem model in many aspects.

6.3. Viscosity

To measure the kinematic viscosity we follow again the method of Dubrulle *et al.* and initialize a flow field $v_x(0) = v_{x0}$ and $v_y(0) = v_{y0} \cos(kx)$ in a system of $60 \times 20 \times 20$ lattice sites with a wavelength of 60 lattice units.

Here we use $v_{x0}=0.1$ and $v_{y0}=0.02$. Then $v_x(t)=v_{x0}$ and the shear wave will decay as

$$v_y(t)=v_{y0}\cos(kx)\exp(-\nu k^2 t) \tag{6.5}$$

The results of the measurements of ν are shown in Figs. 7a and 7b for the unbiased and biased FCHC lattice gas that (a) obeys or (b) violates the Stueckelberg condition, and compared with the predictions from kinetic theory. The viscosity in the latter model is lower than that in the former model, as was to be expected. The biased models were specifically constructed to lower the viscosity. In the model of Fig. 7a the deviations between simulations and theory vary between 0 and 20%, depending on the density. In models of Fig. 7b the deviations for $5<\rho<15$ can be as large as 200%. We recall that in triangular SDB lattice gases the larger part of the difference between simulated and calculated transport coefficients is

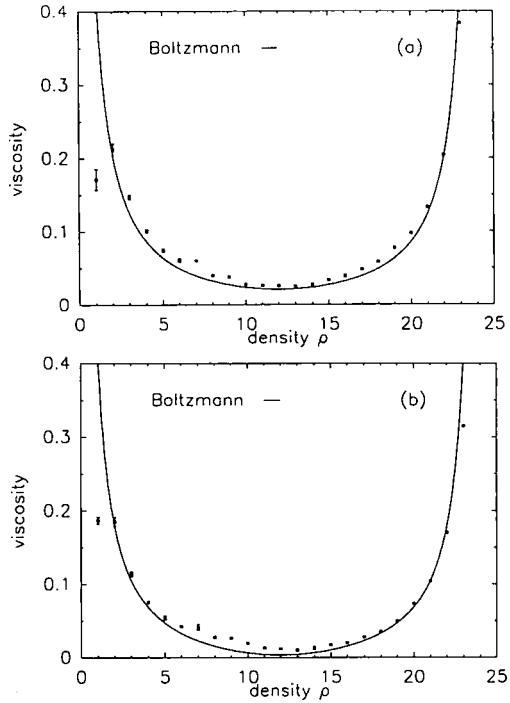

Fig. 7. Viscosity ν versus the density ρ. (a) The semi-detailed balance model; (b) The non-semi-detailed balance model. Solid lines denote the hydrodynamic values, (4.8), while dots represent computer simulations with corresponding error bars.

accounted for by extending the mean field theory to include correlated ring collisions (particles collide, propagate, and recollide again).[38]

We conjecture that the large relative deviations between simulations and mean field theory in biased models will again be accounted for by the ring kinetic equation. This theory not only accounts for dynamic correlations, but also for geometric correlations caused by the slab geometry of the quasi-three-dimensional system.[30] The large deviation at $\rho = 1.0$ is probably caused by a bad signal-to-noise ratio at low density, because of the rather long equilibration times. The system may still be outside the linear regime.

7. CONCLUSIONS

The main achievements of this paper are:

(i) A systematic and compact presentation of the kinetic theory for general FCHC lattice gases with or without rest particles and violating (semi)-detailed balance.

(ii) A geometric interpretation of the extra FCHC symmetry, which is responsible for the isotropy of the viscosity tensor and the nonlinear convective term in the Navier–Stokes equation. This geometric view unequivocally establishes the existence of 12 spurious modes (staggered momentum densities) in all FCHC models with or without rest particles.

(iii) Explicit, compact and transparent expressions for the transport coefficients. We have also emphasized the similarity in structure of the results for continuous gases and lattice gases. In both cases transport coefficients are essentially given in terms of the same matrix elements of the inverse collision operator. The existing unwieldy expressions for the kinematic viscosity ν for FCHC models in refs. 1 and 4 do not exhibit these similarities. The results for the bulk viscosity ζ and for the staggered diffusivities $D_\perp$ and $D_{||}$ are new.

(iv) We have further introduced for the FCHC models generalized hydrodynamics with wavenumber-dependent transport coefficients and relaxation times, which extends linear hydrodynamics to shorter wavelengths. Such extensions are of interest for the study of spatial fluctuations and the dynamic structure function of cellular automata fluids.

(v) To obtain these results we avoid the technicalities of multi-time-scale or Chapman–Enskog methods, and determine the wavenumber-dependent eigenvalues of the linearized Boltzmann equation with spatial dependence. This method is a well-known alternative for calculating transport coefficients in kinetic theory of continuous gases.[31] This paper also extends and generalizes the results of ref. 22 on eigenvalue spectra to

three- and four-dimensional lattice gases. The method is not suitable to derive the nonlinear terms in the Navier–Stokes equations.

(vi) The lattice Boltzmann equation neglects dynamical correlation between velocities of particles on the same and on different sites. In case the semi-detailed-balance conditions are violated, computer simulations show that two-particle velocity distributions do not factorize in the equilibrium state, although the particles are point particles and possess only kinetic energy.

(vii) The predictions of kinetic theory deviate from the predictions of the computer simulations for the speed of sound c_s (up to 3%, well outside the error bars) and for *transport properties* (up to 200%). These observations are consistent with those in ref. 1. We have conjectured in Section 6 that the ring kinetic equation will largely account for the deviations in the transport coefficients.

(viii) We have also compared the simulated speed of sound with the predictions of linear response theory in Section 6.2. They show excellent agreement; those of kinetic theory disagree with the simulation results. All this illustrates indeed that very little is known, even about the equilibrium state, of models that violate the Stueckelberg condition (2.6).

APPENDIX A. COLLISION MATRIX Ω

In this appendix we discuss the linearized collision matrix Ω and calculate its eigenfunctions, as quoted in (3.7), and further properties required for the calculation of transport coefficients. We further show how the special symmetry (2.3) of the FCHC lattice guarantees that the viscosity tensor is isotropic. The matrix Ω is obtained by linearizing the collision term $\mathscr{I}(f+\delta f)$ in the small perturbations δf around the spatially uniform equilibrium state, $f=\rho/24$, i.e.,

$$\mathscr{I}_i(f+\delta f(t))=\sum_j \Omega_{ij}\delta f_j(t)+\mathscr{O}((\delta f)^2) \tag{A.1}$$

The result for single-speed FCHC models with $|\mathbf{c}_j|=\sqrt{2}$ ($j=1, 2,..., b=24$) is[38]

$$\begin{aligned}\Omega_{ij}&=\sum_{s',s}(\delta s_i'-\delta s_i)\,A_{ss'}F_0(s)\,\delta s_j\\&=-\delta_{ij}+\sum_{s',s}\delta s_i'\,A_{ss'}F_0(s)\,\delta s_j\end{aligned} \tag{A.2}$$

$\delta s_j = s_j - f$ and

$$F_0(s) = (f)^{\rho(s)-1}(1-f)^{b-\rho(s)-1} \tag{A.3}$$

where $\rho(s) = \sum_i s_i$ is the number of particles in configuration $\{s(\mathbf{r})\}$ at node $\mathbf{r}$.

In FCHC models without rest particles, the $b \times b$ collision matrix is *symmetric*,

$$\Omega_{ij} = \Omega_{ji} \tag{A.4}$$

on account of the following argument, which is independent of the validity of the Stueckelberg condition. Let p be a lattice isometry that interchanges c_i and c_j. Then lattice symmetries require: if $s \to s'$ with a certain probability, then also $p(s) \to p(s')$ with equal probability for every lattice isometry p, i.e., $A_{ss'} = A_{p(s)\,p(s')}$. Next, we change in (A.2) to new summation variables $s \to p(s)$ and $s' \to p(s')$, and use $(p(s))_j = s_i$, and the symmetry (A.4) follows.

The number of independent matrix elements of Ω can still be reduced further. A matrix element Ω_{ij} is a scalar function of the vectors $\mathbf{c}_i$ and $\mathbf{c}_j$, which depends only on the scalar argument $\mathbf{c}_i \cdot \mathbf{c}_j = 2\hat{\mathbf{c}}_i \cdot \hat{\mathbf{c}}_j \equiv 2 \cos \phi_{ij}$. As $\cos \phi_{ij}$ can only take values 0, $\pm\frac{1}{2}$, ± 1 according to Table I, there are only *five* independent matrix elements for general collision rules with FCHC symmetry. Finally, the conservation laws of mass and momentum give two more independent relations $\sum_i \Omega_{ij} = 0$ and $\sum_i c_{i\alpha} \Omega_{ij} = 0$ for all j. Consequently there are only three independent matrix elements and only *three* independent nonvanishing eigenvalues.

Next we discuss models with additional rest particles, which may or may not follow the Fermi exclusion rule. Then one can show that Ω_{ij} is symmetric, using the weighted inner products of ref. 21, provided the Stueckelberg conditions (2.6) are satisfied. The proof is somewhat involved and will not be given here. If the conditions (2.6) are violated, the matrix Ω is not symmetric.

We consider a model with r rest particles and b moving particles. The basis consists of $r+b$ vectors, each with $r+b$ elements, and the collision operator is an $(r+b)$-dimensional matrix, where the first r entries refer to rest particles and the last b to moving particles. Although Ω is no longer symmetric, it still has the property that $\Omega_{ij} = \Omega_{ji}$ for $\{i, j \in m\}$, where m refers to moving particles, because of the arguments given below (A.4). Also, as all rest particles (r) are equivalent, one verifies that the block matrices $\Omega_{ij} = \varepsilon$, with $\{i \in m, j \in r\}$, and $\Omega_{ij} = \tilde{\varepsilon}$, with $\{i \in r, j \in m\}$, are independent of their labels. Finally, the rest-rest block Ω_{ij} with $\{i, j \in r\}$ has only two different elements, $\Omega_{ii} = \varepsilon_0$ and $\Omega_{ij} = \varepsilon_1$, $i \neq j$, for $\{i, j \in r\}$,

due to the equivalence of rest particles. The Ω matrix has four more elements ($\varepsilon, \varepsilon_0, \varepsilon_1, \tilde{\varepsilon}$), which makes a total of nine independent elements. Conservation laws impose four independent restrictions,

$$\begin{aligned} &\varepsilon_0 + (r-1)\,\varepsilon_1 + b\varepsilon = 0 \\ &\sum_{j\in m} \Omega_{ij} = \sum_{j\in m} \Omega_{ji} = -r\tilde{\varepsilon} \qquad (i \in m) \\ &\sum_{i\in m} c_{i\alpha}\Omega_{ij} = 0 \end{aligned} \tag{A.5}$$

so there are only five nonvanishing eigenvalues.

As the matrix Ω is nonsymmetric, the right and left eigenvectors of Ω, denoted by $\tilde{U}_i$ and U_i, respectively, form a biorthonormal set, i.e., $\langle \tilde{U}_i \mid U_j \rangle = \mathcal{N}_i \delta_{ij}$, where $\mathcal{N}_i$ is a normalization constant. We will use the notation $\tilde{U}_i = (\cdots \,||\, \cdots)$, where the components on the left hand side of the vertical bars refer to rest particles and on the right to the moving particles.

Straightforward calculation yields the $(r+b)$-dimensional eigenvectors $\{U_n, \tilde{U}_m\}$ and eigenvalues ω_n, as defined in (3.5):

$$\left.\begin{aligned} U_1 &= (1,\ldots,1 \,||\, 1,\ldots,1) \\ \tilde{U}_1 &= (\tilde{\varepsilon}/\varepsilon,\ldots,\tilde{\varepsilon}/\varepsilon \,||\, 1,\ldots,1) \end{aligned}\right\} \quad (\omega_1 = 0)$$

$$\left.\begin{aligned} U_2 &= (-b\varepsilon/r\tilde{\varepsilon},\ldots,-b\varepsilon/r\tilde{\varepsilon} \,||\, 1,\ldots,1) \\ \tilde{U}_2 &= (-b/r,\ldots,-b/r \,||\, 1,\ldots,1) \end{aligned}\right\} \quad (\varpi_2 = b\varepsilon + r\tilde{\varepsilon})$$

$$\left.\begin{aligned} U_3 = \tilde{U}_3 &= (1,-1,0,\ldots,0 \,||\, 0,\ldots,0) \\ U_4 = \tilde{U}_4 &= (1,0,-1,\ldots,0 \,||\, 0,\ldots,0) \\ &\vdots \quad\quad \vdots \\ U_{r+1} = \tilde{U}_{r+1} &= (1,0,\ldots,0,-1 \,||\, 0,\ldots,0) \end{aligned}\right\} \quad (\varpi_3 = \varepsilon_1 - \varepsilon_0)$$

$$U_{r+n} = \tilde{U}_{r+n} = (0,\ldots,0 \,||\, u_n) \qquad (\omega_n;\, n = 2,\ldots,b) \tag{A.6}$$

where the relation (A.5) has been used. The b-vectors u_n and eigenvalues ω_n ($n = 1, 2,\ldots, b$) are the same as those listed in (3.7). The eigenvalue ϖ_3 is $(r-1)$-fold degenerate.

If the model satisfies the Stueckelberg conditions (2.6), then Ω is symmetric and $\varepsilon = \tilde{\varepsilon}$. Consequently $U_1 = \tilde{U}_1$ and $U_2 = \tilde{U}_2$. It should also be noted that the matrix elements Ω_{ij} in (A.2) for FCHC models without rest particles depend only on the density through the reduced density $f = \rho/24$. However, if rest particles are included, $F_0(s)$ in (A.3) should be replaced by $F_0(s)/\kappa_j$, where

$$F_0(s) = f_0^{\rho_r(s)}(1-f_0)^{r-\rho_r(s)} f^{\rho_m(s)}(1-f)^{r-\rho_m(s)} \tag{A.7}$$

Here f_0 and f are, respectively, the average occupation number of rest and moving particles with $\rho = rf_0 + bf$. Furthermore, $\rho_r(s) = \sum_{i \in r} s_i$ and $\rho_m(s) = \sum_{i \in m} s_i$ are, respectively, the actual number of rest and moving particles at a node, and $\kappa_j = f_0(1 - f_0)$ if $j \in r$ and $\kappa_j = f(1 - f)$ if $j \in m$. For any given density ρ the stationary distribution f_0 or f must be determined by solving the nonlinear Boltzmann equation, $\mathscr{I}_i(f) = 0$. Using that information as input one can calculate the matrix elements Ω_{ij} and eigenvalues ω_n in (3.7) and (A.6) numerically.

APPENDIX B. BULK VISCOSITY

We calculate the bulk viscosity for a d-dimensional lattice gas with r rest particles and b moving particles with $|\mathbf{c}_i| = c_0$. In FCHC models $c_0 = \sqrt{2}$, in FHP models $c_0 = 1$. The derivation does not depend on the validity or violation of conditions (2.5) or (2.6) and closely parallels that in Section 4.2. However, one should distinguish between right and left eigenvectors. Solving the secular equation to $\mathcal{O}(ik)$ yields instead of (4.6)

$$(z_\sigma^{(1)})^2 = c_s^2 = \frac{\langle c_l \mid c_l \rangle}{\langle U_1 \mid \tilde{U}_1 \rangle} = \frac{c_0^2}{d} \Big/ \left(\frac{r\tilde{\varepsilon}}{b\varepsilon} + 1 \right) \tag{B.1}$$

where U_1 and $\tilde{U}_1$ are defined in (A.6), and ε and $\tilde{\varepsilon}$ in Appendix A, and c_l is an $(r+b)$-dimensional vector with components $c_{li} = 0$ if $|\mathbf{c}_i| = 0$, and $c_{li} = \hat{\mathbf{k}} \cdot \mathbf{c}_i$ if $|\mathbf{c}_i| = c_0$. In SDB models $\tilde{\varepsilon} = \varepsilon$. Consequently, the speed of sound, $c_s = c_0[b/d(r+b)]^{1/2}$, is a universal quantity, independent of the collision rules. However, in NSDB models the speed of sound in (B.1) depends on the details of the collision rules through the Ω-matrix elements ε and $\tilde{\varepsilon}$ defined in Appendix A. Depending on the sign of the ratio $\tilde{\varepsilon}/\varepsilon$, the speed of sound can be larger or smaller than that of an SDB model.

For the viscosity one finds the same expression as in (4.7). The expression for the sound damping constant is slightly modified, i.e.,

$$\Gamma = -\frac{1}{2} \langle c_l^2 - c_s^2 U_1 | \frac{1}{\Omega} + \frac{1}{2} | c_l^2 - c_s^2 \tilde{U}_1 \rangle / \langle c_l \mid c_l \rangle \tag{B.2}$$

With the help of (A.6) the vectors in the above matrix element can be decomposed into two eigenvectors of Ω, i.e.,

$$c_l^2 - c_s^2 U_1 = \left(c_l^2 - \frac{1}{d} c^2 \right) + \left(\frac{1}{2} c_0^2 - c_s^2 \right) U_1 \tag{B.3}$$

and the same relation with U replaced by $\tilde{U}$. The first term corresponds to the eigenvalue $\omega_n = \lambda$ on account of (3.7), and the second one to $\omega_n = \varpi_2 = b\varepsilon + r\tilde{\varepsilon}$, on account of (A.6). Further evaluation of (B.2) yields finally

$$\Gamma = \left(\frac{d-1}{d}\right)\nu + \frac{1}{2}\zeta$$
$$\nu = \frac{c_0^2}{d+2}\left(\frac{1}{\lambda} - \frac{1}{2}\right), \qquad \zeta = \left(\frac{c_0^2}{d} - c_s^2\right)\left(\frac{1}{\varpi_2} - \frac{1}{2}\right) \tag{B.4}$$

In a single-speed model, $c_s = c_0/\sqrt{d}$ and the bulk viscosity vanishes. Also note that the transport coefficients in (B.4) only depend on the number of rest particles through the speed of sound c_s and the eigenvalue ϖ_2.

APPENDIX C. STAGGERED DIFFUSIVITIES

The existence of the staggered mode (2.9) implies that the Boltzmann equations (3.1) and (3.4) have an exact (undamped) solution with period $T = 2$, i.e.,

$$\sum_{r,i} (-1)^{\theta \cdot r}\, \boldsymbol{\theta} \cdot \mathbf{c}_i f_i(\mathbf{r}, t) = \sum_i \boldsymbol{\theta} \cdot \mathbf{c}_i \hat{f}_i(\mathbf{k} = \pi\boldsymbol{\theta}, t)$$
$$= (-1)^t H_\theta = e^{i\pi t} H_\theta \tag{C.1}$$

Here $\hat{f}_i(\mathbf{k}, t)$ is the Fourier transform of the distribution function. Consequently Eq. (4.2) has at wavenumber $\mathbf{k} = \pi\boldsymbol{\theta}$ an exact eigenfunction $\psi(\pi\boldsymbol{\theta}) = \boldsymbol{\theta} \cdot \mathbf{c}$ with eigenvalue $\lambda(\pi\boldsymbol{\theta}) = -1$ or $z(\pi\boldsymbol{\theta}) = \pi i$, i.e.,

$$e^{-i\pi\theta \cdot c}(1 + \Omega)\boldsymbol{\theta} \cdot \mathbf{c} = (-1)^{\theta \cdot c}\, \boldsymbol{\theta} \cdot \mathbf{c} = -\boldsymbol{\theta} \cdot \mathbf{c} \tag{C.2}$$

because all $\boldsymbol{\theta}_j$ satisfy the relation $\boldsymbol{\theta} \cdot \mathbf{c}_i = 0, \pm 1$, as can be seen in Table I.

For wavenumbers close to $\pi\boldsymbol{\theta}$ there exists a *staggered diffusive mode*,

$$\phi_\theta(\mathbf{k}, \mathbf{c}) = \boldsymbol{\theta} \cdot \mathbf{c} \equiv c_\theta$$
$$z_\theta(\mathbf{k}) = \pi i - D_\theta(\hat{\mathbf{k}})\, |\mathbf{k} - \pi\boldsymbol{\theta}|^2 \tag{C.3}$$

with a slowly decaying amplitude $A_\theta(\hat{\mathbf{k}}) = \exp[z_\theta(\mathbf{k})]$, where $D_\theta(\hat{\mathbf{k}})$ is the staggered diffusivity. By perturbation expansion around $\phi_\theta^{(0)} = c_\theta$ and $z_n^{(0)} = \pi i$, we obtain the result (4.10) for the anisotropic staggered diffusivity. According to (4.11), it can be split into a longitudinal and a transverse part,[17,39] given by

$$D_{\parallel} = -\langle c_\theta^2 | \frac{1}{\Omega + \Delta(c_\theta)} + \frac{1}{2} | c_\theta^2 \rangle / \langle c_\theta | c_\theta \rangle$$
$$D_{\perp} = -\langle c_\theta c_{t\alpha} | \frac{1}{\Omega + \Delta(c_\theta)} + \frac{1}{2} | c_\theta c_{t\alpha} \rangle / \langle c_\theta | c_\theta \rangle \tag{C.4}$$

where $c_{t\alpha} = \mathbf{e}_\alpha(\boldsymbol{\theta}) \cdot \mathbf{c}$ and $\{\boldsymbol{\theta}, \mathbf{e}_\alpha(\boldsymbol{\theta}); \alpha = 1, 2, 3\}$ form an orthogonal set of unit vectors.

To evaluate these expressions, we may choose $\boldsymbol{\theta} = (1, 0, 0, 0)$ (see Table I), because all reciprocal lattice vectors are equivalent and related by lattice symmetries. Then $c_\theta c_{\perp\alpha} = c_x c_y$ is a common eigenfunction of Ω and $\Delta(c_\theta)$ with eigenvalues $-\lambda$ and 0, respectively, and the transverse diffusion coefficient becomes $D_\perp = \nu$, as quoted in (4.11). To calculate $D_{\parallel}$ we deduce from the symmetries of Ω and $\Delta(c_x)$ that

$$[\Omega + \Delta(c_x)]^{-1} c_x^2 = A + B c_x^2 \tag{C.5}$$

Straightforward calculation gives then $A = 1/2$ and $B = -2/\lambda$. Substitution of (C.5) in (C.4) yields finally $D_{\parallel} = 6\nu$, as quoted in (4.11).

ACKNOWLEDGMENTS

The authors thank J. W. Dufty for valuable criticism that led to the linear response results of Section 6.2 and M. Hénon for valuable suggestions and comments on an earlier version of the manuscript. R.B. acknowledges support by DGICYT (Spain) under contract number PB91-0378 and a grant of the Ministerio de Educación (Spain).

REFERENCES

1. B. Dubrulle, U. Frisch, M. Hénon, and J. P. Rivet, *J. Stat. Phys.* **59**:1187 (1990).
2. M. Hénon, *J. Stat. Phys.* **68**:353 (1992).
3. J. A. Somers and P. C. Rem, in *Lecture Notes in Physics*, Vol. 398, T. M. M. Verheggen, ed. (Springer-Verlag, Berlin, 1992), p. 59.
4. M. Hénon, *Complex Syst.* **1**:475 (1987).
5. U. Frisch, D. d'Humières, B. Hasslacher, P. Lallemand, Y. Pomeau, and J. P. Rivet, *Complex Syst.* **1**:649 (1987).
6. J. F. Olson and D. H. Rothman, in *Pattern Formation and Lattice-Gas Automata*, A. Lawniczak and R. Kapral, eds. (American Mathematical Society, to be published).
7. C. Appert and S. Zaleski, in *Pattern Formation and Lattice-Gas Automata*, A. Lawniczak and R. Kapral, eds. (American Mathematical Society, to be published).
8. N. G. van Kampen, *Stochastic Processes in Physics and Chemistry* (North-Holland, Amsterdam, 1981).
9. E. C. G. Stueckelberg, *Helv. Phys. Acta* **25**:577 (1952); W. Heitler, *Ann. Inst. H. Poincaré* **15**:67 (1956).

10. H. J. Bussemaker and M. H. Ernst, *J. Stat. Phys.* **68**:431 (1992).
11. D. H. Rothman and J. M. Keller, *J. Stat. Phys.* **52**:1119 (1988).
12. D. H. Rothman, *J. Stat. Phys.* **56**:517 (1989).
13. C. Appert, D. H. Rothman, and S. Zaleski, *Physica D* **47**:85 (1991).
14. F. J. Alexander, I. Edrei, P. L. Garrido, and J. L. Lebowitz, *J. Stat. Phys.* **68**:497 (1992).
15. H. J. Bussemaker and M. H. Ernst, *Physica A* **194**:258 (1993).
16. M. Gerits, M. H. Ernst, and D. Frenkel, *Phys. Rev. E* **48**:988 (1993).
17. M. H. Ernst and J. W. Dufty, *J. Stat. Phys.* **58**:57 (1990).
18. J. A. Somers and P. C. Rem, in *Cellular Automata and the Modelling of Complex Systems*, P. Manneville, ed. (Springer, 1989), p. 161.
19. G. Westland, Master's thesis, State University of Utrecht (1991), unpublished.
20. P. G. Grosfils, J. P. Boon, and P. Lallemand, *Phys. Rev. Lett.* **68**:1077 (1992).
21. P. G. Grosfils, J. P. Boon, R. Brito, and M. H. Ernst, *Phys. Rev. E* **48**: (1993).
22. S. P. Das, H. J. Bussemaker, and M. H. Ernst, *Phys. Rev. E* **48**:245 (1993).
23. G. Zanetti, *Phys. Rev. A* **40**:1539 (1989).
24. M. H. Ernst, in *Liquids, Freezing and the Glass Transition, Les Houches, Session LI, 1989*, D. Levesque, J. P. Hansen, and J. Zinn-Justin, eds. (Elsevier, Amsterdam, 1991), p. 43.
25. T. Naitoh, M. H. Ernst, and J. W. Dufty, *Phys. Rev. A* **42**:7187 (1990).
26. M. Hénon, in *Pattern Formation and Lattice-Gas Automata*, A. Lawniczak and R. Kapral, eds. (American Mathematical Society, to be published).
27. M. A. van der Hoef and D. Frenkel, *Phys. Rev. A* **41**:4277 (1990).
28. M. A. van der Hoef, M. Dijkstra, and D. Frenkel, *Europhys. Lett.* **17**:39 (1992).
29. M. Hénon, *Complex Syst.* **1**:763 (1987).
30. R. Brito and M. H. Ernst, *Phys. Rev. A* **44**:8384 (1991).
31. P. Resibois and M. de Leener, *Classical Kinetic Theory of Fluids* (Wiley, New York, 1977).
32. S. Chapman and T. G. Cowling, *The Mathematical Theory of Nonuniform Gases* (Cambridge University Press, Cambridge, 1970).
33. T. R. Kirkpatrick and M. H. Ernst, *Phys. Rev. A* **44**:8051 (1991).
34. S. H. Luo, H. Chen, S. Chen, G. D. Doolen, and Y. C. Lee, *Phys. Rev. A* **43**:7097 (1991).
35. H. J. Bussemaker and M. H. Ernst, in Cagliari Proceedings Workshop Cagliari, September 1992, S. Succi, ed., *Stat. Phys. Transport Theory* (1993).
36. R. Brito and M. H. Ernst, *J. Stat. Phys.* **62**:283 (1991).
37. D. van Coevorden, Master's thesis, State University of Utrecht (1992), unpublished.
38. G. A. van Velzen, R. Brito, and M. H. Ernst, *J. Stat. Phys.* **70**:811 (1993).
39. R. Brito and M. H. Ernst, *J. Phys. A* **24**:3331 (1991).